Article

Time Series and Spectral Analysis of Thermoacoustic Oscillations for Propane-Oxyfuel Combustion in a Swirl-Stabilized, Nonpremixed Combustor

Qazi Talal, Zubairu Abubakar, M. Raghib Shakeel, Mohammed Saad AlSwat, and Esmail M.A. Mokheimer*

Cite This: ACS Omega 2023, 8, 36053−36064

Read Online

ACCESS | Metrics & More | Article Recommendations

ABSTRACT: In this study, the time series data for sound pressure and heat release fluctuations were analyzed to establish the stability window of the propane-oxyflames under different operating conditions. The CO_2 dilution level and the combustor power density were varied at a fixed global equivalence ratio to investigate the thermoacoustic instability of the flames. The phase difference between the fluctuations and the instantaneous Rayleigh index reveals whether the heat release and pressure fluctuations are coupled, which can result in the amplification of the sound pressure fluctuations. Results showed a negative Rayleigh index and uncoupled fluctuations at low (<40%) and high (>60%) CO_2 dilution with coupled fluctuations and sound pressure amplification at intermediate CO_2 dilution levels. A peak of varying magnitude appeared in the frequency domain at 465 Hz for both the heat release and pressure fluctuations in the coupled mode. The Strouhal number at different CO_2 concentrations revealed a range of vortex-shedding frequencies (300−1000 Hz), suggesting that the coupled mode is vortex-induced. Phase space reconstruction for the sound pressure fluctuations was carried out and it is observed that although the pressure fluctuations are amplified in the coupled mode, limit cycle amplitudes have not been reached. The recorded coupling and uncoupling of the oscillations associated with flame-vortex interactions at certain CO_2 concentrations provides a valuable insight on the combustor's dynamics and toward the development of nonpremixed-oxy-flames combustors.

1. INTRODUCTION

The combustion of fossil fuels contributes to around 85% of the total energy produced globally. The advantages of fossil fuels regarding energy and power density make them very difficult to replace in the near future. Burning of fossil fuels results in the production of soot, unburned hydrocarbons, CO_2, CO, SO_x, and NO_x that significantly contribute to environmental pollution. Combustion-generated pollutants lead to acid rain, smog, and greenhouse gases, which cause global warming and climate change. Greenhouse gases including carbon dioxide, water vapors, and trace amounts of other gases such as methane, O_3, CFC, HFC, and HCFC act like a blanket and block the heat radiated from the earth, thus leading to global warming. Increasingly, stringent legislation is being enacted in the industrialized world to control the quantity of pollutants generated by most combustion sources.

It is important for researchers in combustion technology to investigate different technologies to decrease the emissions that adversely affect the environment. Hydrogen combustion or the combustion of hydrates like ammonia (a means of hydrogen storage) is among the carbon-free fuel under study

by many researchers.[1,2] Furthermore, ways of mitigating NOx emissions from this and other carbon-free combustion systems that are air-oxidized is actively under study.[3,4] Recently, carbon capture and storage (CCS) has been broadly looked at as a way to decrease the emissions caused by greenhouse gases. Compared to air-oxidized systems, up to 80−90% in CO_2/kWh reduction can be achieved by employing CCS.[5] Various CCS technologies have been recommended and developed.[6,7] The different classifications of CCS include oxyfuel combustion, precombustion, or postcombustion capture.[8] In oxy-combustion, oxygen is used as an oxidizer in place of traditionally used air for combustion of the fuel. However, flames oxidized by pure oxygen are characterized by temper-

atures higher than those of air-oxidized flames. Recirculation of cooler exhaust gases may be necessary to lower the oxy-combustion temperatures. CO_2 and H_2O are produced from pure oxygen combustion. Water vapor can be condensed and removed from the exhaust gas mixture so that CO_2 can be sequestered. An oxidizer mixture composed of recycled gases can be mixed with oxygen to control the flame temperature and to compensate for the absent N_2 volume (available in an air oxidizer). Since the nonrecycled CO_2 is sequestered and NOx formation is not an issue associated with oxy-combustion, CCS can be regarded as a combustion process with zero carbon and NOx emissions.[9]

The other general complication associated with combustion is combustion instabilities. Combustion instabilities can result in damage to the combustor and subsequent explosion. While combustion instability is well researched in air-oxidized combustion systems, it is essential to equally develop the literature for oxy-combustion. The word instability character-izes scenarios in which minor input disruptions in initial or boundary conditions result in an intense reaction, leading to the output of the system dramatically changing or expanding to larger amplitudes. A new system state, which is typically very different from the original state, is formed after a transition time. In many circumstances, a total collapse of the original condition is seen.

There are two types of combustion instabilities: static instabilities and dynamic instabilities. Flame flashback and blowout are the phenomena responsible for static instability. Flashback happens when the speed of flow surpasses the speed of flame. In the cases when the speed of the flame is higher than the speed of flow, it leads to the occurrence of blowout of the flame. Another scenario also occurs due to the coupling of heat release and acoustic pressure variations, which are categorized as dynamic instabilities, also known as thermoa-coustics, resulting in the generation of undesirable pressure waves in the surrounding environment. These instabilities are problematic because they can create unnecessary excess noise and reduce operation capability and can also result in significant structural damage. Thermoacoustic instabilities have been studied widely for air-oxidized premixed systems; however, a smaller number of studies are available for nonpremixed systems, especially with oxyfuel combustion. Some of those studies are reviewed below.

The literature regarding combustion stability can be broadly classified into those focusing on the stability at different mixture concentrations (CO_2 diluent in O_2/CO_2 oxidizer mixtures in case of oxy-combustion), the effect of the combustor geometry, the effect of the flow-field interactions with flame, and those focusing on control strategies. The operating limits and combustion instability with varying oxygen percentage were investigated by Li.[10] Oxyfuel methane combustion was carried out in a swirl-stabilized burner, with the oxygen concentration in the O_2/CO_2 mixtures ranging from 25 to 100%. The stable flame region occurs for the conditions at which oxygen mole fraction is less than 50%, from lean-flame to rich-flame conditions. When the oxygen mole fraction is greater than 60%, fluctuation occurs at stoichiometric and rich equivalence ratios. A combustion-driven oscillation with a high frequency (about 2000 Hz) was reported in the study. Oxy-combustion instabilities and emission characteristics at different O_2/CO_2 mixtures were also investigated by Li et al.[11] in a stabilized combustor. A significant impact was observed due to varying the oxygen

concentration in the O_2/CO_2 oxidizer mixtures. The study identified a strong relationship between concentration of oxygen and combustion delay. Strong oscillations in the oxy-combustion cases were observed to dampen at higher oxygen concentrations. Furthermore, the study reports that compared to the air-fueled cases, the oxyfuel cases had a much higher temperature level producing a larger amount of carbon monoxide. Abubakar and Mokheimer[12] experimentally inves-tigated a nonpremixed swirl stabilized combustor for oxyfuel combustion. The mixture used in the study was propane and propane-hydrogen with CO_2 dilution in an oxygen oxidizer. The different parameters that were varied were the firing rate of the combustor, hydrogen concentration in propane, and CO_2 dilution level. The results indicated that instability was triggered at 45% carbon dioxide dilution, amplified at 50%, and damped above 60% dilution. Increasing the concentration of hydrogen and decreasing the firing rate also resulted in a decrease in the sound pressure and heat release amplitude. The study conducted in this study further analyzed the thermoacoustic instability mechanisms for propane oxyfuel combustion within the swirl-stabilized combustor. Other literature focusing on the oxy-combustion thermoacoustic instability at different mixture dilutions in O_2/CO_2 oxidizer mixtures include these studies as well.[13−16]

Zhou et al.[17] investigated the influence of the geometry of the combustor on the response of the nonpremixed flame under acoustic stimulation. Among the geometric alterations are the lengths of the combustor intake sections, which are set at 0.243, 0.333, and 0.440, 0.333, and 0.440 m, respectively, in addition to the placement of separating plates. When the excitation frequency was varied, the greatest fluctuations responded around 144 Hz for the 0.345 and 0.245 m cases, respectively. It is reported in the study that fuel pipe resonance was responsible for this mode. Li[10] studied different-sized slits for fuel injection into a swirl-stabilized combustor with different-sized slit widths used to enhance fuel-oxidizer mixing. It is reported that the stability window of the combustion was significantly increased by lowering the width of the slit through which the fuel flows to half of the slit through which the oxidizer flows. Consequently, it is suggested that at high oxygen concentrations associated with strong oscillations, narrowing the fuel intake breadth and generating a higher speed of injection are necessary for stable flames.

Kang and Culick[18] studied the response of the flow field of air-fuel mixture to induced sound fluctuations at frequencies of 22, 27, 32, 37, and 55 Hz. It is reported that a close relationship exists between the mixture fraction of the fuel distribution within the zone of mixing, which is predicted to grow into the equivalence ratio, and the behavior of the flame that is both unstable and oscillatory. The mixture fractions were seen to oscillate at similar frequency values as the driving frequency but with an additional difference in phase. It was therefore concluded that the oscillation of the mixture fractions was most probably the primary cause of the oscillations. Within a nonpremixed flame, the effect of acoustic coupling on the combustion behavior was investigated by Tyagi et al.[19] In a uniform flow field, a 2D coflow combustion model was studied for the nonpremixed flame. The chemistry effects were studied for two types of mechanisms: infinite and finite rate mechanisms. At different frequency values, the effect of external velocity oscillation on the coupled flame response was studied. For varying velocity oscillations, the phase and amplitude of heat release oscillations were determined, and it

was found that these values were crucially affected by the Damköhler number. Baraiya and Chakravarthy[20] carried out a study on thermoacoustic instability within a turbulent nonpremixed combustor investigating the effect of syngas composition. The Reynolds number (Re) was varied from 2200 to 8100 to investigate the acoustics in three syngas compositions: pure hydrogen and a mixture of hydrogen with methane. The instability occurred at a unique frequency of 130 Hz for the hydrogen-methane mixture; however, for the pure hydrogen and all three syngas compositions, two modes of thermoacoustic instability were observed for the entire range of Re. Within the shear layer of the bluff body, the occurrence of the flame significantly modulated the high-frequency acoustic excitation, as shown by the spatial-temporal analysis of the time-resolved data.

Studies focusing on combustion instability control include Snarheim et al.[21] in which the oxy-flames were modeled and linear analysis was carried out. A control-relevant model was built by employing CO_2 as the working medium. The analysis on the newly built model revealed that secondary CO_2 injection near the flame is a more easily managed factor compared with the injection of fuel to control fluctuations. Magnetic fields were utilized by Jocher[22] to minimize combustion instabilities. In an interdisciplinary study that merged electromagnetics and combustion, the researchers discovered a novel and fundamental experiment that demonstrated spontaneous flame instability that was alleviated when the nonpremixed sooting flame was exposed to a magnetic disturbance. This control strategy results from momentum and thermochemistry coupling that was maintained by the magnetic force, which acted primarily on paramagnetic oxygen in this case. It was discovered by the spatial local stability analysis based on numerical simulations that the magnetic field decreased the growth rates of tiny flame disturbances in a spatially localized manner. Idahosa[23] investigated the reaction of swirling nonpremixed flames in the presence of sound at different frequency values ranging from 0 to 315 Hz and different swirl intensities. A coflow burner was studied, for which acoustic fluctuations were generated using a loudspeaker, and the ensuing amplitudes of velocity fluctuation had a range from 0.03−0.30. Through the investigation of different flame configurations at constant values of the fuel flow rate, it was discovered that there is an effect of flame dynamics on the comparative richness of the flame. For identifying underlying processes that are common to highly sensitive flame designs, methods for phase conditioning, Rayleigh criteria, wavelet analysis, and the acoustic impedance approach were applied.

This study is aimed at extending the analysis of thermoacoustic instability mechanisms for propane oxyfuel combustion at different CO_2 dilution levels in a swirl-stabilized combustor as reported by Abubakar and Mokheimer.[12] Phase space reconstruction of the acoustic and heat release time series is carried out. The instantaneous Rayleigh index and the oscillation's phases at different CO_2 dilution levels are presented to identify coupled and uncoupled modes. Furthermore, the relation between the Reynolds number and the Strouhal number is utilized to relate the observed fluctuations to the flow characteristics. These additional analyses carried out in the current study deepened our understanding of the thermo-acoustic stability of oxyfuel combustion with the CO2 diluent in the nonpremixed combustor. Furthermore, this study contributes to the evolving literature on oxycombustion toward green energy transformation.

2. EXPERIMENTAL SETUP

Figure 1 illustrates the schematic diagram of the experimental setup. Combustion is carried out by burning nonpremixed
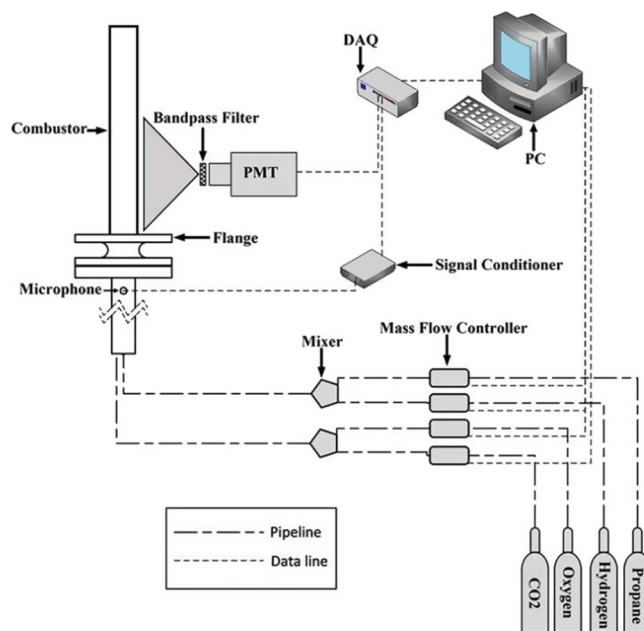

Figure 1. Detailed experimental setup is represented by a schematic diagram.

propane and oxidizer in the burner at atmospheric pressure conditions. Compressed gas cylinders are used to supply propane, oxidizer (oxygen), and diluent (carbon dioxide) having a purity of 99.9%. The oxidizer and diluent are mixed by using a mixing chamber before entering the combustor. The reactants are supplied to the combustor by using a Bronkhorst High-Tech mass flow controllers. The detailed geometry of the burner is illustrated in Figure 2. The burner geometry and experimental setup are discussed in detail in the previous study.[12]

In this experiment, the sound pressure oscillations are measured by high-intensity microphones (MIC-093) manufactured by Kulite semiconductor products Inc. The microphone measures dynamic pressure with a dynamic range of 100 to 194 dba, a sensitivity output of 9 mV (nominal) at 160 dba,
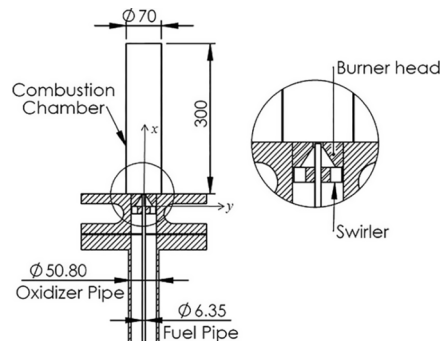

Figure 2. Detailed representation of the burner geometry (all dimensions in mm).

and a temperature range of −55 to 260 °C. The microphone is installed upstream of the combustor dump plane by flush mounting, as indicated in Figure 1. The fuel pipe and the oxidizer pipe are concentric with the outer pipe containing the oxidizer mixture and the pressure measuring sensor. For controlling factors such as gain and overload, a signal conditioner has been used in combination with microphones to obtain the acoustic pressure fluctuations.

The intermediate combustion radicals emit light in a specific spectral band, which can be used as a heat release marker. However, this chemiluminescence from excited radicals like OH*, CH*, and C_2* cannot be adequately used to quantitatively measure flame heat release. This is particularly true for carbonaceous fuels where broadband of CO_2* (275 to >513 nm) can superimpose onto the narrowband emissions (OH*, CH*, and C_2*; narrow spectral band of 308, 431, and 513 nm, respectively).[24] Band-pass filtered measurement, therefore, can only be used without correction to measure the relative integral intensity of the intermediate radicals that is proportional to an integral heat release rate. This type of measurement has been carried out for thermoacoustic stability analysis in nonpremixed flames[25−29] and distributed flames[13,14] in different studies. Furthermore, the ratio OH*/CH* is reported to be employed in the determination of the local equivalence ratio in both premixed and nonpremixed flames.[26,30,31] In this study, OH* chemiluminescence is measured by a photomultiplier tube module (PMT), model H10722−110, manufactured by Hamamatsu Photonics UK Ltd. The PMT is used along with an OH* bandpass filter at 307 ± 5 nm wavelength for targeting OH* radicals manufactured by Optosigma, USA. The PMT is placed normal to the flame at a fixed distance such that the entire flame is captured by the PMT, as illustrated in Figure 1.

The data obtained for the acoustic pressure and heat release measurements are fed into a data acquisition system from National Instruments (NI) and are recorded by using LABVIEW software. The data were collected for 10 s at a sampling frequency of 10 kHz. For each condition, 100,000 data points were recorded in this study. All experiments were carried out at atmospheric pressure and ambient temperature conditions. Spectral analysis of the data obtained was done by using the Fast Fourier Transform (FFT) technique. This technique was used to convert the acoustic pressure and heat release fluctuation values from the time domain to the frequency domain in order to identify the peak amplitudes and frequencies.

The effect of CO_2 dilution on thermoacoustic instability is studied in a nonpremixed swirl combustor for propane-oxy-combustion. The CO_2 % in the oxidizer was varied from 0% up to the percentage at blowout. The global equivalence ratio was fixed at 1 for all experiments. The impact of varying the power density of the combustor was also investigated in this study. The equation below represents the power density of the combustor:

$$\text{Combustor power density} = \frac{m_f \times \text{LHV}}{V_c P_c} \tag{1}$$

In the equation fuel lower heating value is denoted by LHV (46 MJ/kg C_3H_8), pressure of the combustor in bar is represented by P_c, volume of the combustor in m^3 is denoted by V_c, and fuel mass flow rate is expressed by m_f having the unit kg/s.

The operating conditions are illustrated in Table 1 below:

Table 1. Operating Conditions of This Study

parameters	combustor power density (MW/m³ bar)	global equivalence ratio, Φ	CO₂ concentration in oxidizer
Carbon dioxide dilution	4.0	1	0−77% (blowout)
Combustor firing rate	3.0, 3.5, 4.5	1	50%

3. RESULTS AND DISCUSSION

3.1. Time Series and FFT of Pressure and Heat Release at Varying CO_2 Dilution. The effect of CO_2 dilution on thermoacoustic instability is studied in a non-premixed swirl combustor for propane-oxy-combustion. The experiments were started at 100% oxygen concentration with no CO_2 dilution, following which the CO_2 % in the oxidizer was increased until the flame blowout occurred. Figure 3 illustrates the time series spectra for sound pressure and heat release oscillations and the corresponding FFTs in the frequency domain for varying the CO_2 dilution from 0 to 45%. At 0 and 20% dilution, it can be observed, from the time series spectra, that the heat release fluctuations have a very small magnitude; hence, it does not excite any peaks in the sound pressure spectra as is evident from the FFT spectra, indicating that the flame is stable without any presence of thermoacoustic instability.

At 45% CO_2 dilution, the time series spectra show that the magnitude of heat release fluctuations is very high, and at this point, thermoacoustic instability onset occurred, as can be observed in the sound pressure FFT graph with a peak being present at 465 Hz. However, the heat release fluctuations are completely out of phase with the pressure time spectra; hence, the heat addition fluctuations damp the acoustic pressure field, which is evident from the appearance of a very low amplitude peak within the sound pressure spectra. The high magnitude heat release fluctuations also occur at low frequencies and do not excite any acoustic modes of the combustor at those low frequencies.

Figure 4 depicts the time series spectra for acoustic pressure and heat release oscillations as well as the FFT's in the frequency domain for varying the CO_2 dilution from 50 to 65%. At 50% CO_2 dilution, the time series spectra show that the magnitude of heat release oscillations decreased compared to the previous case of 45%; however, the phase difference between the sound pressure and heat release is much smaller, and as such, the sound pressure fluctuations are amplified. The amplified sound pressure fluctuations occurring at 465 Hz also excite, at identical frequency, a peak in the heat release fluctuations, indicating that coupling has occurred in the combustor between the sound pressure and the subsequent heat release peak and thus the feedback loop is initiated, resulting in significant thermoacoustic instability within the combustor. At 60% CO_2 dilution, the phase difference between the sound pressure and heat release peaks is very small, and as such, the peaks in both the spectra are amplified to the maximum value in the combustor, indicating the highest thermoacoustic instability among all experimental conditions. The phase difference between the pressure and heat release time series increases again at 65% CO_2 dilution, which results
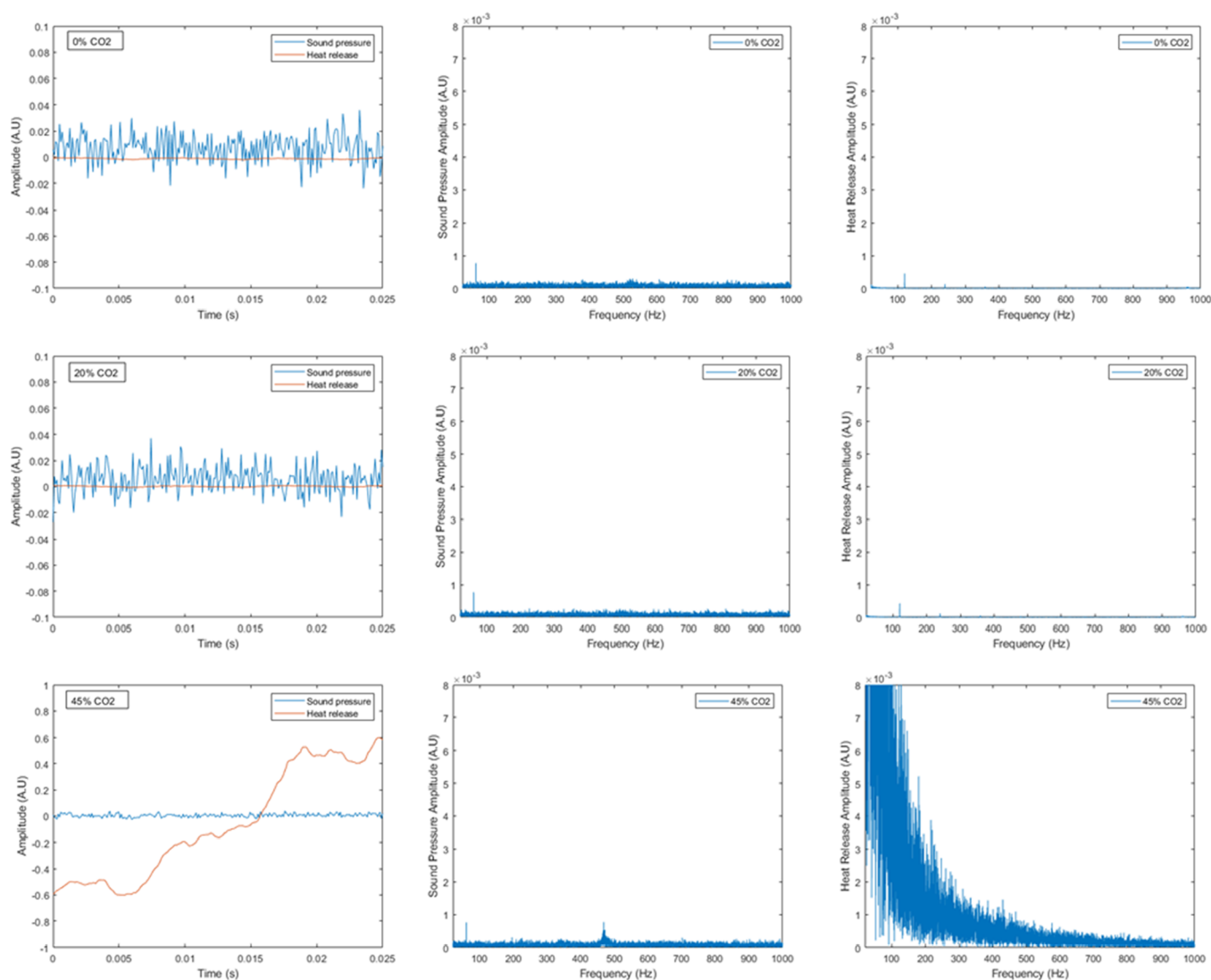
Figure 3. Pressure and heat release time series data and FFT for varying the CO_2 concentration (0−45%) at power density 4 MW/m^3 bar.

in the damping of the sound pressure oscillations field, and the subsequent damping effect on the heat release fluctuation was observed as well, indicating the decrease in instability magnitude within the combustor. Another interesting observation as the CO_2 dilution increases, the heat release fluctuations magnitude occurring at lower frequencies also diminishes, which were very high at 45% CO_2 dilution.

Figure 5 illustrates the time series spectra for acoustic pressure and heat release oscillations as well as the FFT's in the frequency domain at a CO_2 dilution of 69% and at 77% (blowoff). At 69% CO_2 dilution, the time series spectra show that sound pressure and heat release oscillations have a much larger phase difference; hence, the heat addition oscillations dampen the acoustic field, removing energy from the acoustic field, resulting in a very low amplitude peak in the pressure spectra. The energy losses become higher, and the subsequent heat release peak has a much lower amplitude and is not distinguishable in the heat release spectra indicating the decoupling of the sound pressure and heat release. Near the blowout point at 77% CO_2 dilution, the pressure and heat release are out of phase, and as such, the heat release fluctuations do not excite any acoustic modes. However, the occurrence of several low amplitude peaks can be observed in

the pressure spectra, and this is due to the partial flame extinction or vortex convecting through the nozzle which occurs usually near the blowout points. These mechanisms excite an acoustic wave that propagates back to the flame exciting another convective wave and thus repeating the process.

3.2. Phase Space Reconstruction of Pressure and Heat Release Data. Phase space reconstruction has been used in several studies[32,33] to identify whether the combustor is in unstable condition and has reached limit cycle amplitudes. Phase space reconstruction is used to carry out nonlinear time-series analysis[34] in order to study the dynamics of the system evolving over time. The phase space cannot be reconstructed directly as the state variables are unknown and instead must be reconstructed with "Takens time-delay embedding theorem".[35] Time series data obtained from experiments can be used with the Takens time-delay embedding theorem to obtain a phase space reconstruction and analyze the stability of the system under study. In this study, heat release and pressure time series data recorded from experiments are used. Numerical algorithms developed for the Takens theorem in MATLAB called the Average Mutual Information (AMI) and False Nearest Neighbor (FNN) are used. There are two main
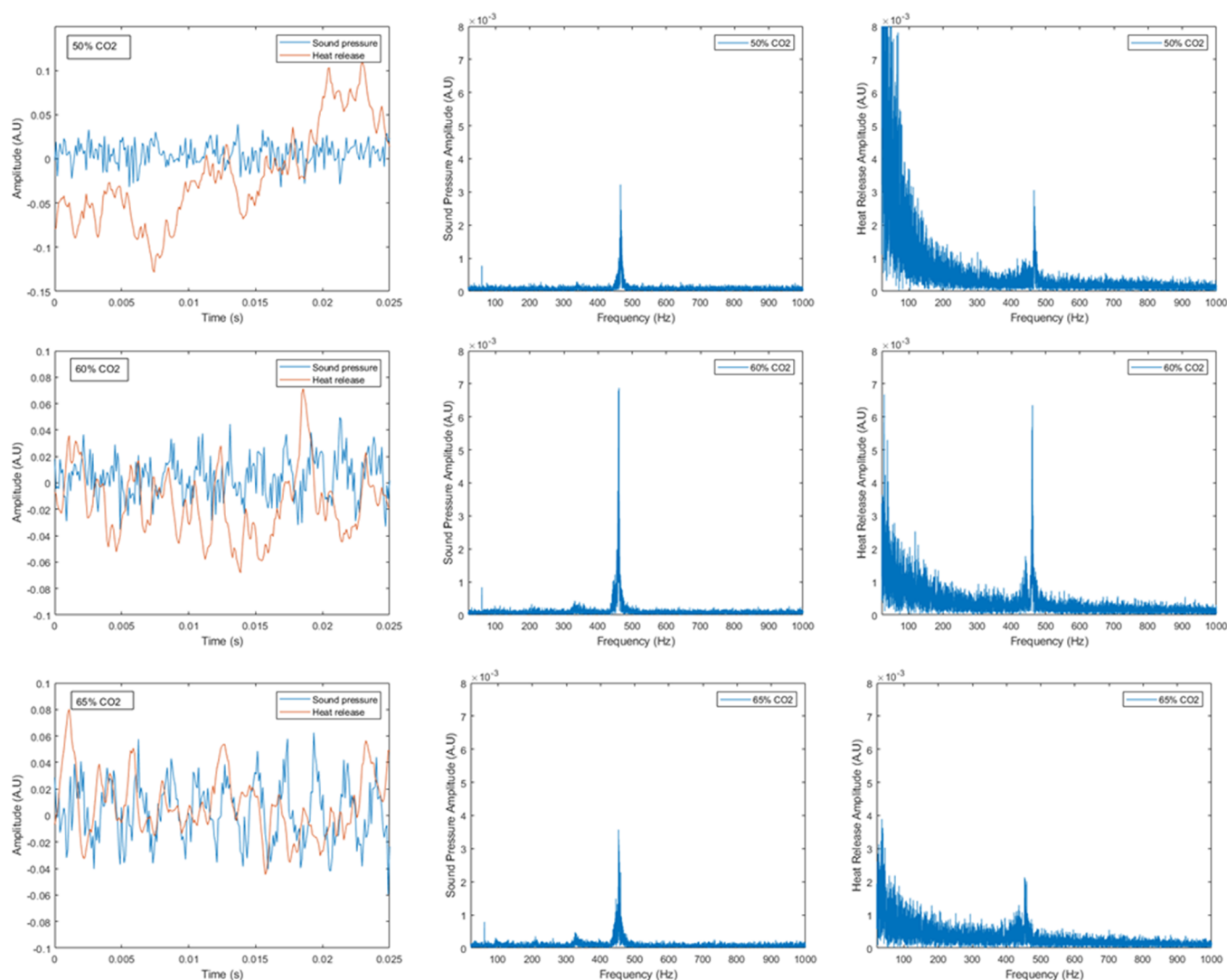
Figure 4. Pressure and heat release time series data and FFT for varying CO_2 concentration (50−65%) at a power density 4 MW/m^3 bar.

parameters required for carrying out phase space reconstruction, which are the time delay and embedding dimension estimated by AMI and FNN, respectively. The detailed mathematical expressions for AMI and FNN can be found in the references.[34,36]

Figure 6 illustrates the phase space reconstruction[37,38] of the sound pressure fluctuations time series for varying CO_2 dilution. For a phase space reconstruction plot, stable or unstable conditions are ascertained by the compactness or growth of the time series data plotted. Subsequently, a variation in the size of the phase plot from small and compact to a larger distribution entails the growth of instability. This growth, when is represented by pressure fluctuation data in a combustor, can represent a transitional state to instability or even unstable conditions.[32] For limit cycle oscillations, the phase space reconstruction plots will have a larger distribution with a hollow region at the center of the distribution.[32,33]

It can be observed from Figure 6 that the pressure fluctuation distribution starts to grow at 50% CO_2 dilution, as evident from the larger distribution of the phase plot at that CO_2 concentration. This is the point at which coupling and amplification of sound pressure occur. The largest distribution is observed at 60% CO_2, which agrees with the observation for

obtaining the highest amplitude peaks in the sound pressure spectra. Following this, the pressure distribution starts to decrease from 65% CO_2 dilution onward as the pressure oscillations are damped gradually, until at 77% CO_2 dilution near blowoff, where the pressure distribution is similar to pressure distributions at 0% CO_2 dilution. The pressure fluctuations under coupled conditions from 50 to 69% CO_2 dilution illustrate a transition state between stable and unstable modes as represented by the growth of the distributions in the phase plots; however, as limit cycle amplitudes were not reached, the combustor had not reached completely saturated unstable conditions. Consequently, while the pressure fluctuations are amplified at 50−60% CO_2 percentages, limit cycle amplitudes have not been reached in the combustor and the oscillations are dampened at higher CO_2 concentrations.

Figure 7 illustrates the phase space reconstruction of the heat release fluctuation time series for varying CO_2 dilution. The heat release fluctuations obtained from this analysis agree with the time series data at 0 and 20% dilution with the phase space plots showing very minute distribution, indicating that the magnitude of heat release fluctuations under those conditions are very low. At 45% dilution, the largest distribution for heat release fluctuation can be observed
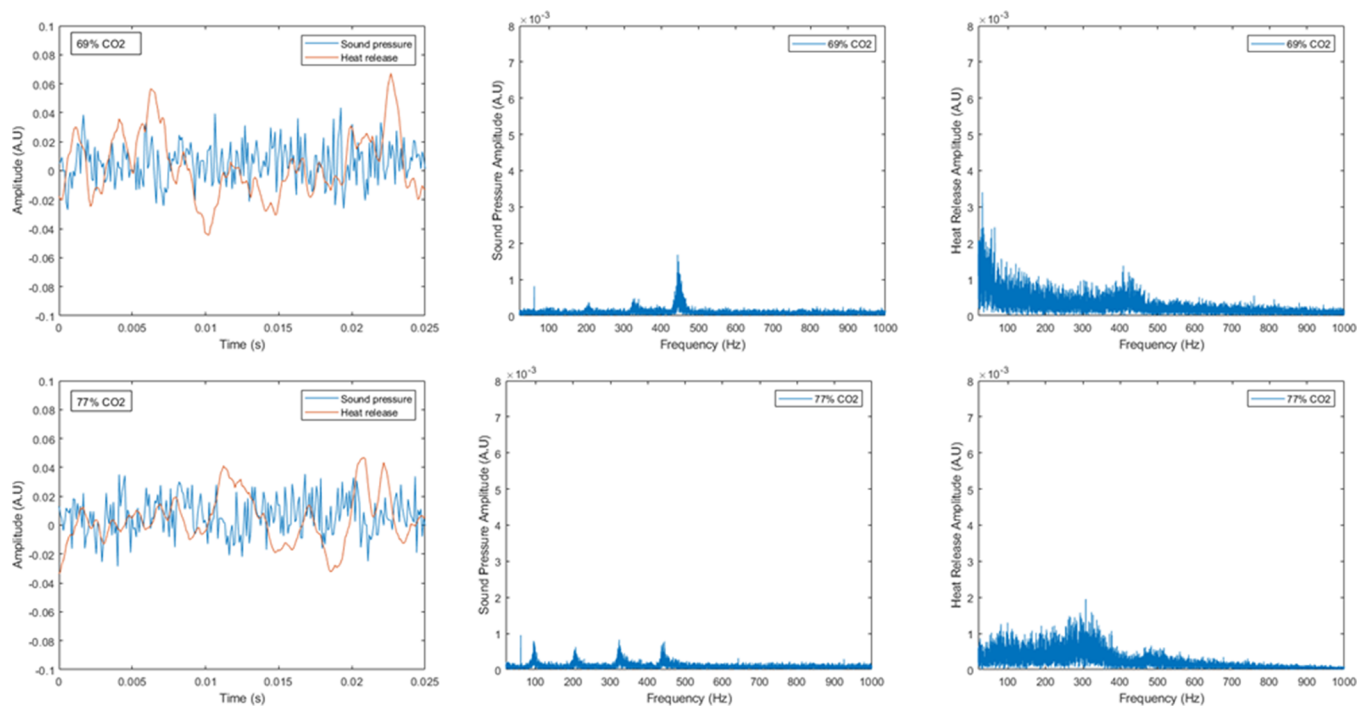
Figure 5. Pressure and heat release time series data and FFT for varying CO_2 concentration (69%, 77%) at power density 4 MW/m^3 bar.
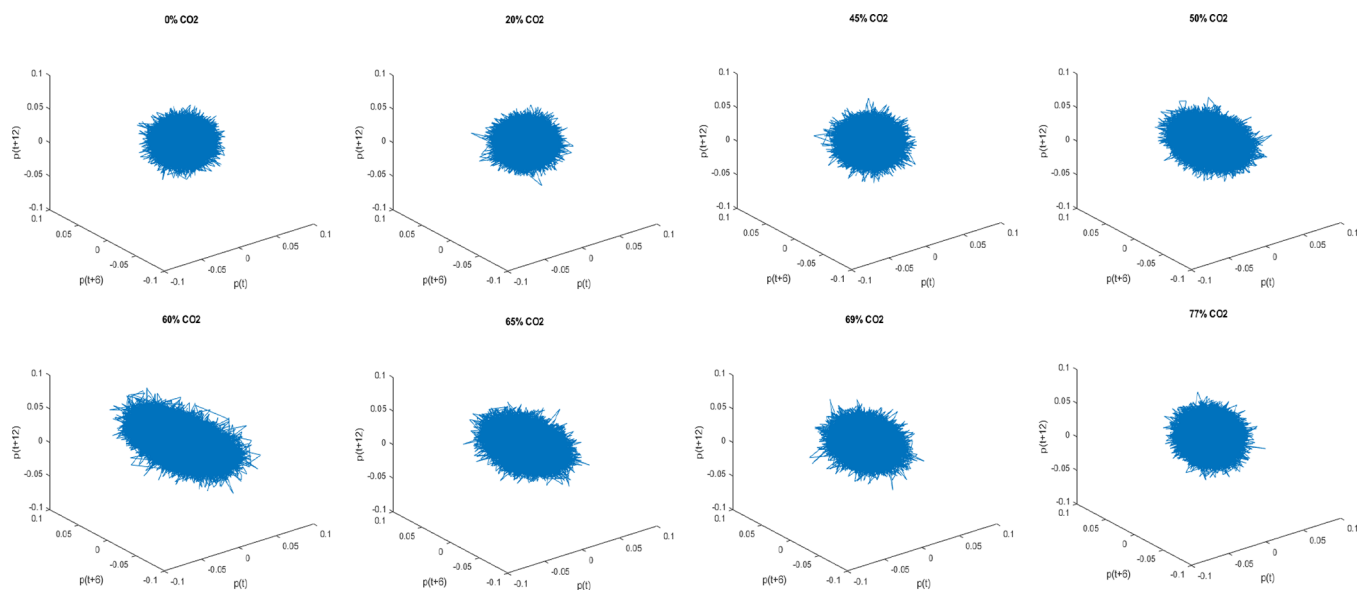

Figure 6. Phase space reconstruction of pressure signals at varying CO_2 concentrations at power density 4 MW/m^3 bar.

which was evident from the FFT spectra due to the heat release fluctuations that occurred at low frequency. The heat release distributions decrease in magnitude as CO_2 dilution increases, and this can be related to the previous observation that the low-frequency fluctuations decrease in magnitude with an increase in CO_2 dilution. From 60% CO_2 dilution onward, the influence of low-frequency magnitudes is substantially suppressed, and the heat release phase space plots represent the damping of heat release fluctuations as CO_2 dilution reaches near blowout.

3.3. Time Series, FFT, and Phase Space Reconstruction of Pressure and Heat Release at Different Combustor Power. The impact of varying combustor power density had been investigated at a constant value of

50% CO_2 dilution. Figure 8 illustrates the time series plots and FFT and phase space plots at a power density of 3 MW/m^3 bar. The time series spectra show that although the magnitude of heat release fluctuations is quite high, the heat release fluctuations are completely out of phase with the pressure time spectra hence the heat addition fluctuations damp the acoustic pressure field, which is evident from the appearance of very low amplitude peak in the pressure spectra. The sound pressure peak hence does not excite any subsequent peak in the heat release spectra. The heat release oscillations occur at low frequencies and do not excite any acoustic modes of the combustor at those low frequencies. The phase space plot for the sound pressure data also illustrates a small collapsed distribution, indicating that significant acoustic instability has
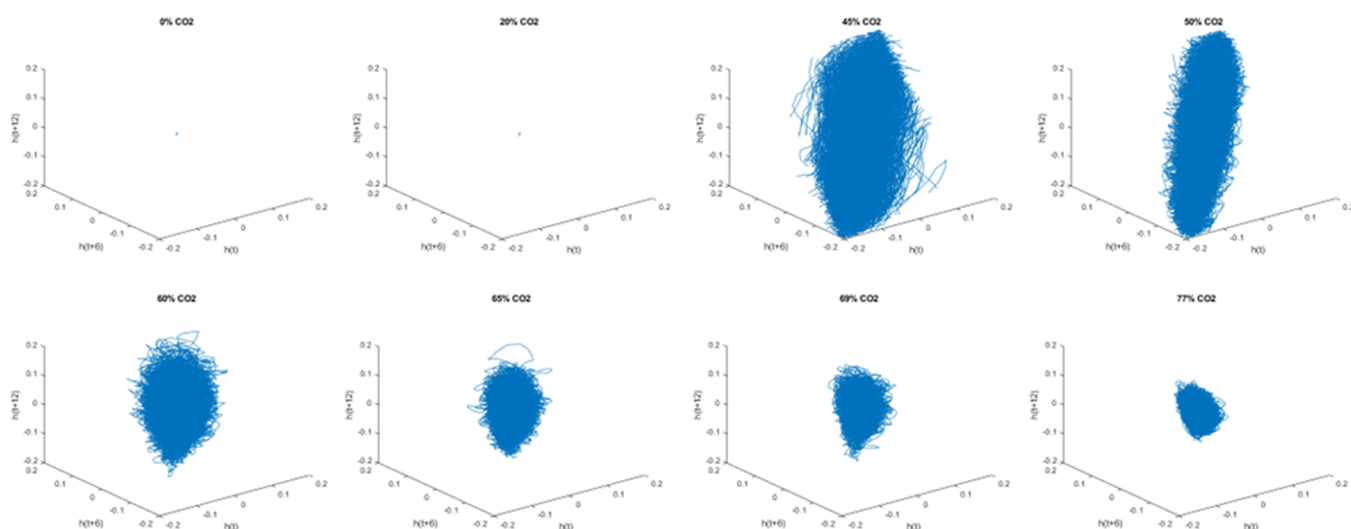
Figure 7. Phase space reconstruction of heat release signal at varying CO_2 concentration at power density 4 MW/m³ bar.
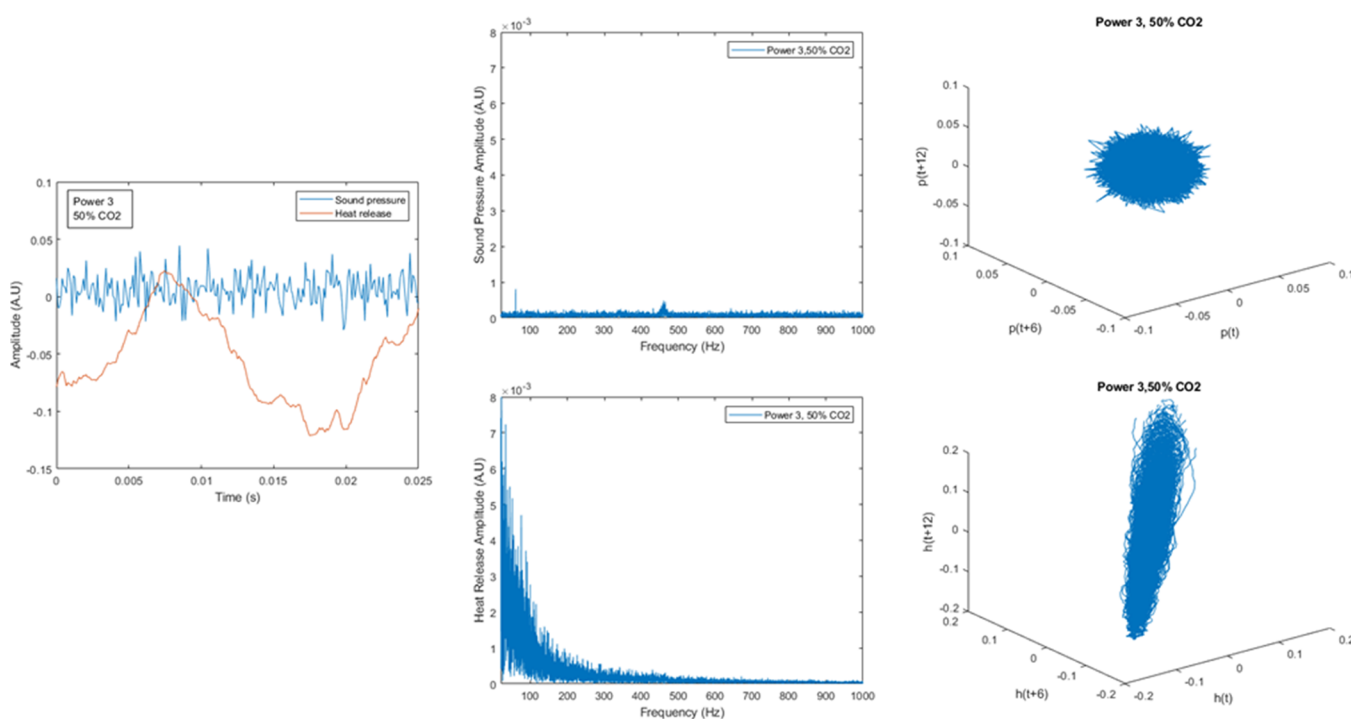

Figure 8. Pressure and heat release time series data (left), spectral analysis with FFT (middle), phase space reconstruction (right) at 50% CO_2 concentration, and combustor power density = 3 MW/m³ bar.

not occurred yet for this dilution % at lower combustor power. The heat release phase space plot shows a large distribution, but the magnitude of the heat release oscillations occurred at the lower frequencies.

Figure 9 illustrates the time series plots, FFT, and phase space plots at a power density of 3.5 MW/m³ bar. At this condition, the time series spectra show that the phase difference between the sound pressure and heat release is smaller compared to the previous condition, and as such, the sound pressure fluctuations are amplified. The amplified sound pressure fluctuations occurring at 460 Hz also excite a peak at an identical frequency in the heat release fluctuations, indicating that coupling has occurred in the combustor between the sound pressure and the subsequent heat release peak, and thus, the feedback loop is initiated, resulting in

thermoacoustic instability within the combustor. Compared to Figure 8, the pressure phase space plot also shows a growth in the distribution, indicating the amplification of acoustic instability. The heat release phase space plot shows a decrease in distribution compared to the condition at 3 MW/m³ bar, as although peak coupling occurs at this condition, the fluctuations at low frequency were smaller, which is mainly contributing to the distribution of the heat release phase space plot.

Figure 10 illustrates the time series plots and FFT and phase space plots at a power density of 4.5 MW/m³ bar. Under this condition, the phase difference between the sound pressure and heat release peaks is very small. Consequently, the peaks in both the spectra are amplified to the maximum value at this dilution condition indicating high thermoacoustic instability.
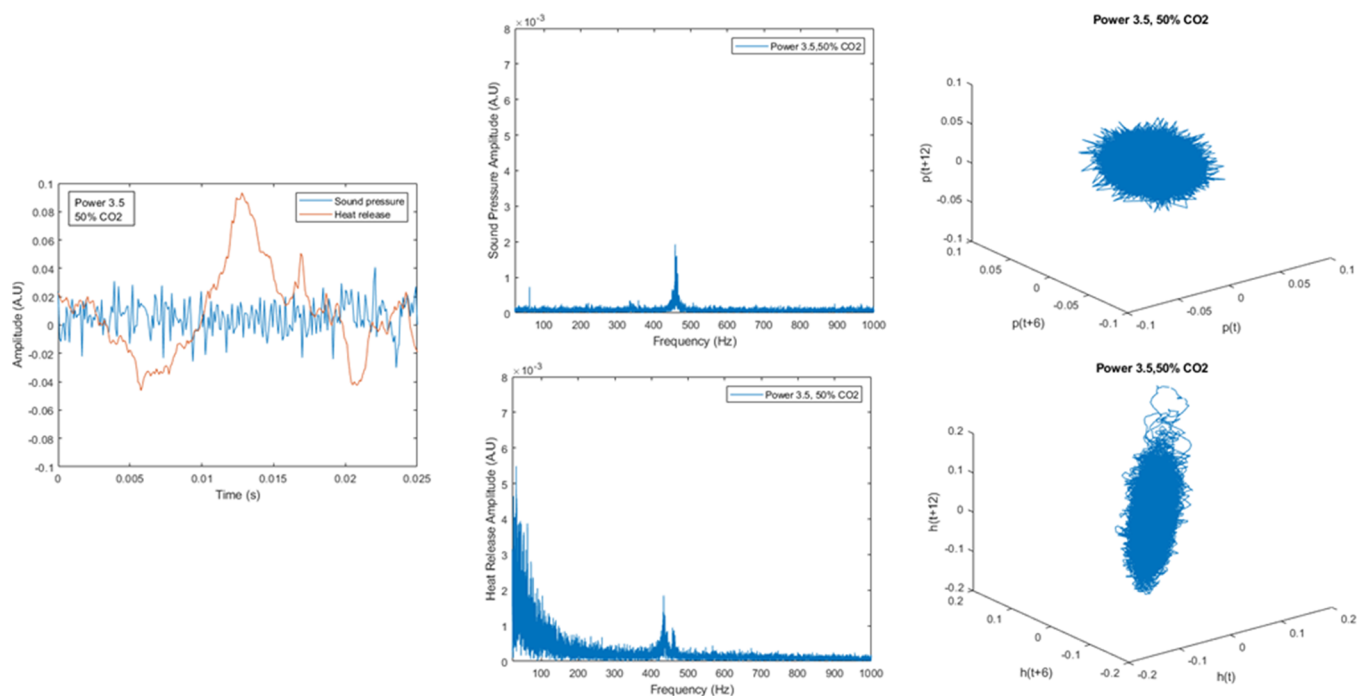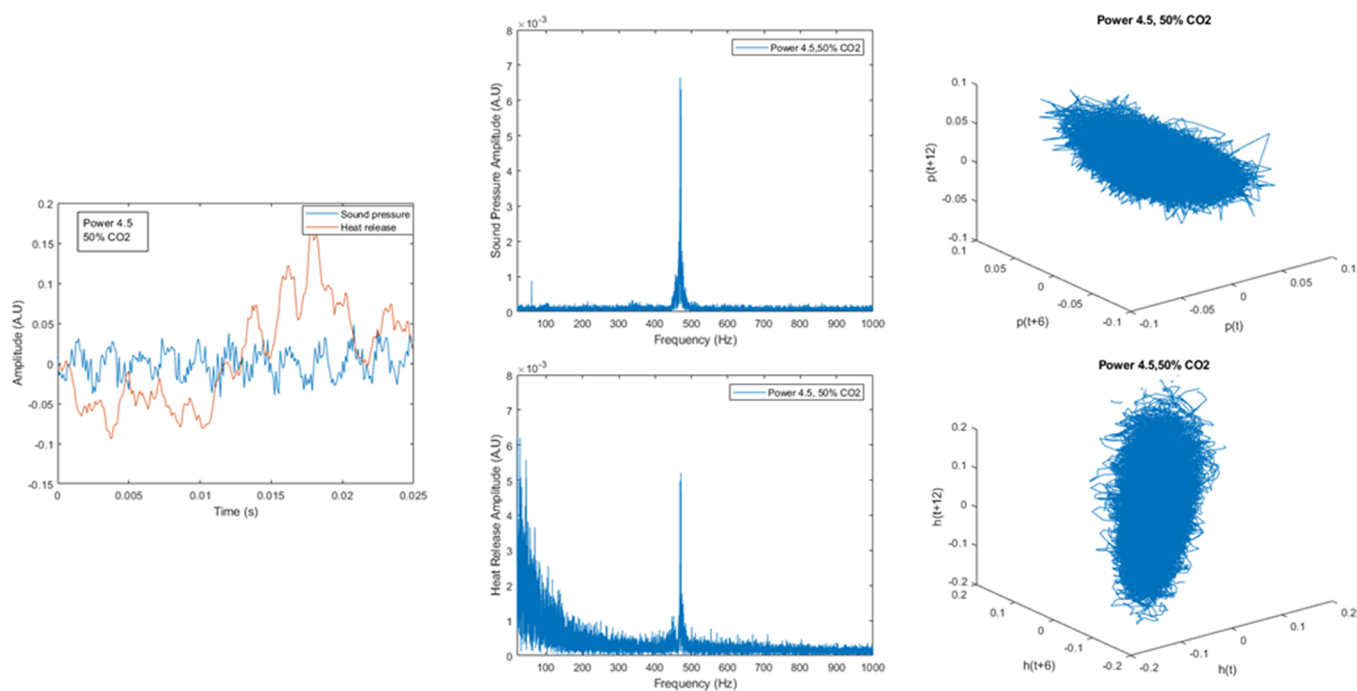
Figure 9. Pressure and heat release time series data (left), spectral analysis with FFT (middle), phase space reconstruction (right) at 50% CO_2 concentration, and combustor power density = 3.5 MW/m^3 bar.

Figure 10. Pressure and heat release time series data (left), spectral analysis with FFT (middle), phase space reconstruction (right) at 50% CO_2 concentration, and combustor power density = 4.5 MW/m^3 bar.

The frequency of the coupled peaks however shifts to a higher value of 470 Hz due to higher velocities at higher combustor power density. The phase space plot for the pressure data shows a significant growth in the pressure distribution compared with Figures 8 and 9, indicating that the acoustic fluctuations are very unstable at this higher power density. The heat release phase space plot similarly shows a much larger distribution as well representing the high magnitude of the heat release fluctuations under coupled conditions.

3.4. Flame Rayleigh Index. The Rayleigh index helps provide important information regarding thermoacoustic coupling. It is given by the following expression:

$$RI = \frac{1}{T} \int_0^T p' q' \, dt \tag{2}$$

In this expression, p and q are fluctuations of pressure and heat release, respectively, and T is the calculation period. The pressure and heat release data from the experiments were used

to estimate the Rayleigh index by numerically integrating the data using eq 2. Figure 11 represents the Rayleigh index for
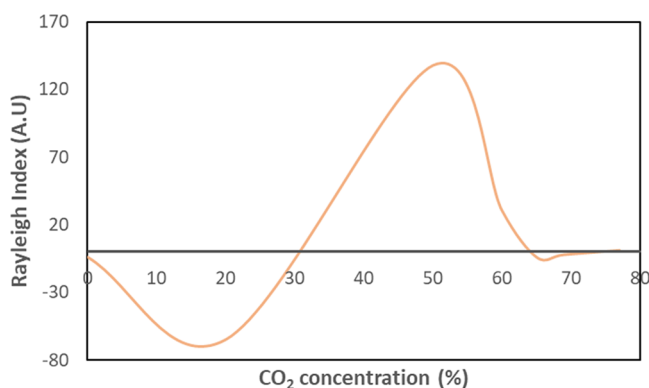

Figure 11. Flame Rayleigh Index as a function of CO_2 concentration at combustor power density = 4 MW/m^3 bar.

varying the CO_2 concentration from 0% (pure oxygen) to 77% (blowout) at a combustor power density of 4 MW/m^3 bar under stoichiometric conditions. From 0% up to 30%, the Rayleigh index has a negative value which denotes uncoupled oscillations and damping of thermoacoustic oscillations. At higher CO_2 concentration, near 50% where coupling of pressure and heat release fluctuation occurs and subsequent amplification of thermoacoustic instabilities occurs, positive values are observed for the Rayleigh Index, indicating that thermoacoustic instabilities are amplified. As the CO_2 concentration is increased to 65% and then to 69%, the Rayleigh index drops to a negative value again, indicating the damping of thermoacoustic oscillations under these conditions. This can be observed from Figures 4 and 5 as well, where under these conditions, the acoustic pressure and heat release oscillation amplitude decrease as the CO_2 concentration increases.

3.5. Frequency of Vortex Shedding Obtained from Strouhal Number−Reynolds Number Correlation. The relationship between the Reynolds number (Re) and the Strouhal number (St) was developed by Vincent Strouhal (1878) and is given by the following expression:

$$St = fL/U \tag{3}$$

In the equation, the flow velocity is given by U, the characteristic length is denoted by L, and the vortex shedding frequency is represented by f. The Strouhal number can also be estimated using an empirical correlation:[39,40]

$$St = 0.198(1 - 19.7/Re) \tag{4}$$

This formula is valid for the range of $250 < Re < 2 \times 10^5$. At large values of the Reynolds number, the Strouhal number is, thus, approximately constant. The vortex shedding frequency can then be estimated using the expression in eq 3.

Figure 12 represents the range of vortex shedding frequencies calculated for varying CO_2 concentration from 0 to 77% (blowout) at a combustor power density of 4 under stoichiometric conditions. The flow velocities were calculated at different CO_2 dilution values, and Reynolds number values were obtained. The Strouhal number was approximated and corresponding vortex shedding frequencies were calculated.
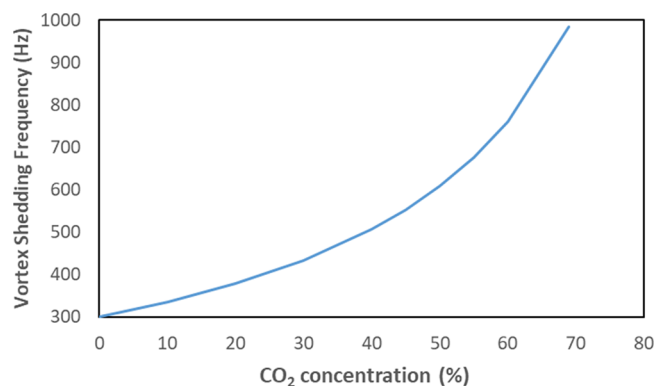

Figure 12. Vortex shedding frequency as a function of the CO_2 concentration.

The vortex shedding frequencies range from 300 to 1000 Hz, which is dependent mainly on the flow velocities (and hence, Reynolds number), which increased with an increase in the volume of CO_2 added to the oxidizer. In the experiments carried out for combustor power density 4 MW/m^3 bar, the peak frequency at which coupling of sound pressure and heat release occurred was 465 Hz which is within the range of frequencies obtained from the analytical calculations. This suggest that the thermoacoustic instability observed is vortex-induced.

4. CONCLUSIONS

Experiments were carried out for a nonpremixed swirl stabilized combustor for oxyfuel combustion with propane. The CO_2 dilution level and the power density of the combustor were varied to investigate the thermoacoustic instability of propane-oxyfuel flames. The time series data for sound pressure and heat release fluctuations were analyzed for varying conditions to identify the phase difference between the fluctuations and whether the heat release fluctuations amplify or dampen the sound pressure fluctuations. At low CO_2 dilution levels, the heat release oscillations dampened the acoustic field, but at higher CO_2 dilution levels from 50 to 60%, the heat release oscillations amplified the sound pressure amplitudes reaching peak instability conditions. As the dilution levels were further increased to 65% up to the blowout of the flame the heat release fluctuations dampened the acoustic field until the sound pressure and heat release oscillations were decoupled. The spectral analysis of the fluctuations in the frequency domain revealed the magnitude of the peak frequency and amplitude under coupled conditions. Phase space reconstruction for the sound pressure fluctuations was carried out to identify if the combustor reached unstable mode and limit cycle amplitudes. No limit cycle amplitudes were observed in the sound pressure spectra, however, the growth of the pressure distributions illustrated a transition state for the combustor between stable and unstable modes. The phase space plots for the heat release oscillations illustrated the magnitude of the fluctuations at varying dilution levels. The impact of the power density of the combustor was also investigated at 50% CO_2 dilution, and the results were illustrated through time series, FFT, and phase space reconstruction plots. As the combustor power density increased amplification in thermoacoustic instability was observed with a slight shift in the frequency of peak coupling. The flame Rayleigh index for varying CO_2 dilution levels was

calculated to illustrate the damping and amplification of thermoacoustic instability for propane-oxyfuel flames. Results showed a negative Rayleigh index and uncoupled fluctuations at low (<40%) and high (>60%) CO_2 dilution level with coupled fluctuations and sound pressure amplification at intermediate CO_2 dilution levels. Finally, the vortex shedding frequencies were determined to identify and correlate the peak frequency coupling occurring in this experimental investigation. The Strouhal number at different CO_2 concentrations revealed a range of vortex-shedding frequencies (between 300−1000 Hz) suggesting that the coupled mode is vortex-induced.

■ AUTHOR INFORMATION

Corresponding Author

Esmail M.A. Mokheimer − *Mechanical Engineering Department and Interdisciplinary Research Center for Renewable Energy and Power Systems (IRC-REPS), King Fahd University of Petroleum & Minerals, Dhahran 31261, Saudi Arabia; Senior Researcher, K.A. CARE Energy Research and Innovation Center, Dhahran 31261, Saudi Arabia;* ● orcid.org/0000-0002-5774-8517; Email: esmailm@kfupm.edu.sa

Authors

Qazi Talal − *Mechanical Engineering Department, King Fahd University of Petroleum & Minerals, Dhahran 31261, Saudi Arabia*

Zubairu Abubakar − *Mechanical Engineering Department, University of Tabuk, Tabuk 71421, Saudi Arabia*

M. Raghib Shakeel − *Mechanical Engineering Department, King Fahd University of Petroleum & Minerals, Dhahran 31261, Saudi Arabia;* ● orcid.org/0000-0001-7539-3492

Mohammed Saad AlSwat − *Mechanical Engineering Department, University of Tabuk, Tabuk 71421, Saudi Arabia*

Complete contact information is available at:
https://pubs.acs.org/10.1021/acsomega.3c04144

Notes

The authors declare no competing financial interest.

■ ACKNOWLEDGMENTS

■ REFERENCES

(1) Li, J.; Huang, H.; Deng, L.; He, Z.; Osaka, Y.; Kobayashi, N. Effect of hydrogen addition on combustion and heat release characteristics of ammonia flame. *Energy* **2019**, *175*, 604−617.

(2) Katoch, A.; Guiberti, T. F.; de Campos, D. V.; Lacoste, D. A. Dual-fuel, dual-swirl burner for the mitigation of thermoacoustic instabilities in turbulent ammonia-hydrogen flames. *Combust. Flame* **2022**, *246*, No. 112392.

(3) Cai, T.; Zhao, D.; Gutmark, E. Overview of fundamental kinetic mechanisms and emission mitigation in ammonia combustion. *Chem. Eng. J.* **2023**, *458*, No. 141391.

(4) Cai, T.; Zhao, D.; Ji, L.; Agarwal, A. K. Removal and mechanism analysis of NOx emissions in carbon-free ammonia combustion systems with a secondary fuel injection. *Fuel* **2023**, *344*, No. 128088.

(5) Rubin, E. S.; Chen, C.; Rao, A. B. Cost and performance of fossil fuel power plants with CO2 capture and storage. *Energy Policy* **2007**, *35*, 4444−4454, DOI: 10.1016/j.enpol.2007.03.009.

(6) Cuéllar-Franca, R. M.; Azapagic, A. Carbon capture, storage and utilisation technologies: A critical analysis and comparison of their life cycle environmental impacts. *J. CO2 Util.* **2015**, *9*, 82−102, DOI: 10.1016/j.jcou.2014.12.001.

(7) Figueroa, J. D.; Fout, T.; Plasynski, S.; McIlvried, H.; Srivastava, R. D. Advances in CO2 capture technology-The U.S. Department of Energy's Carbon Sequestration Program. *Int. J. Greenh. Gas Control* **2008**, *2*, 9−20.

(8) Jordal, K.; Anheden, M.; Yan, J.; Strömberg, L. "Oxyfuel combustion for coal-fired power generation with CO2 capture—Opportunities and challenges," Rubin, E. S.; Keith, D. W.; Gilboy, C. F.; Wilson, M.; Morris, T.; Gale, J.; K. B. T.-G. G. C. T., Thambimuthu, Eds.; Elsevier Science Ltd: Oxford, 2005; 201−209.

(9) Richards, G. A.; Casleton, K. H.; Chorpening, B. T. CO2 and H2O diluted oxy-fuel combustion for zero-emission power. *Proc. Inst. Mech. Eng. Part A J. Power Energy* **2005**, *219* (2), 121−126. Mar.

(10) Li, B.; et al. Oxy-fuel combustion of methane in a swirl tubular flame burner under various oxygen contents: Operation limits and combustion instability. *Exp. Therm. Fluid Sci.* **2018**, *90*, 115−124.

(11) Li, G. N.; Zhou, H.; Cen, K. F. Emission characteristics and combustion instabilities in an oxy-fuel swirl-stabilized combustor. *J. Zhejiang Univ. Sci. A* **2008**, *9* (11), 1582−1589.

(12) Abubakar, Z.; Mokheimer, E. M. A. Thermoacoustic combustion instability of propane-oxy-combustion with CO2 dilution: Experimental analysis. *Int. J. Energy Res.* **2020**, *44* (2), 1031−1045. Feb.

(13) Khalil, A. E. E.; Gupta, A. K. Acoustic and heat release signatures for swirl assisted distributed combustion. *Appl. Energy* **2017**, *193*, 125−138.

(14) Khalil, A. E. E.; Gupta, A. K. Flame fluctuations in Oxy-CO2-methane mixtures in swirl assisted distributed combustion. *Appl. Energy* **2017**, *204*, 303−317.

(15) Kutne, P.; Kapadia, B. K.; Meier, W.; Aigner, M. Experimental analysis of the combustion behaviour of oxyfuel flames in a gas turbine model combustor. *Proc. Combust. Inst.* **2011**, *33* (2), 3383−3390.

(16) Ditaranto, M.; Hals, J. Combustion instabilities in sudden expansion oxy−fuel flames. *Combust. Flame* **2006**, *146* (3), 493−512.

(17) Zhou, H.; Meng, S.; Tao, C.; Liu, Z. Study of burner geometry effects on non-premixed flame response under acoustic excitation. *J. Low Freq. Noise Vib. Act. Control* **2019**, *38* (1), 3−17.

(18) Kang, D.; Culick, F.; "An experimental study of coupling between combustor pressure, fuel/air mixing, and the flame," *4th Jt. Meet. U.S. Sect. Combust. Institute*, 2005.

(19) Tyagi, M.; Chakravarthy, S. R.; Sujith, R. I. Unsteady combustion response of a ducted non- premixed flame and acoustic coupling. *Combust. Theory Model.* **2007**, *11* (2), 205−226.

(20) Baraiya, N. A.; Chakravarthy, S. R. ScienceDirect Effect of syngas composition on high frequency combustion instability in a non-premixed turbulent combustor. *Int. J. Hydrogen Energy* **2019**, *44* (12), 6299−6312.

(21) Snarheim, D.; Imsland, L.; Foss, B. A. Control-relevant modelling and linear analysis of instabilities in oxy-fuel combustion. *2007 Eur. Control Conf. ECC* **2007**, *2007*, 3568−3575.

(22) Jocher, A.; et al., "Combustion instability mitigation by magnetic fields To cite this version: HAL Id: hal-01557986," 2017, DOI: 10.1103/PhysRevE.95.063113.

(23) Idahosa, U. O., "Combustion dynamics and fluid mechanics in acoustically perturbed non-premixed swirl stabilised flames," 2010.

(24) Lauer, M. R. W., "Determination of the heat release distribution in turbulent flames by chemiluminescence imaging;" Tech. Univ: München, 2011.

(25) Idahosa, U.; Saha, A.; Xu, C.; Basu, S. Non-premixed acoustically perturbed swirling flame dynamics. *Combust. Flame* **2010**, *157* (9), 1800−1814.

(26) Lauer, M.; Sattelmayer, T. On the Adequacy of Chemiluminescence as a Measure for Heat Release in Turbulent Flames With Mixture Gradients. *J. Eng. Gas Turbines Power* **2010**, *132* (6), No. 061502. Mar.

(27) Merotto, L.; Sirignano, M.; Commodo, M.; D'Anna, A.; Dondè, R.; De Iuliis, S. Experimental Characterization and Modeling for Equivalence Ratio Sensing in Non-premixed Flames Using Chemiluminescence and Laser-Induced Breakdown Spectroscopy Techniques. *Energy Fuels* **2017**, *31* (3), 3227−3233. Mar.

(28) Chi, Y.; Lei, Q.; Song, E.; Fan, W.; Sha, Y. Development and Validation of Evaluation Methods for 3D Flame Propagation Speed of Turbulent Non-premixed Edge Flames via Tomographic Chemiluminescence. *Flow, Turbul. Combust.* **2022**, *108* (2), 539−557.

(29) Eckart, S.; Yu, C.; Maas, U.; Krause, H. Experimental and numerical investigations on extinction strain rates in non-premixed counterflow methane and propane flames in an oxygen reduced environment. *Fuel* **2021**, *298*, No. 120781.

(30) Panoutsos, C. S.; Hardalupas, Y.; Taylor, A. M. K. P. Numerical evaluation of equivalence ratio measurement using OH∗ and CH∗ chemiluminescence in premixed and non-premixed methane−air flames. *Combust. Flame* **2009**, *156* (2), 273−291.

(31) Wäsle, H.; Winkler, A.; Lauer, M.; Sattelmayer, T.; "Combustion noise modeling using chemiluminescence data as indicator for the heat release distribution," in *3rd European Combustion Meeting*, 2007.

(32) Han, X.; Laera, D.; Morgans, A. S.; Sung, C. J.; Hui, X.; Lin, Y. Z. Flame macrostructures and thermoacoustic instabilities in stratified swirling flames. *Proc. Combust. Inst.* **2019**, *37* (4), 5377−5384.

(33) Han, X.; et al. Flame interactions in a stratified swirl burner: Flame stabilization, combustion instabilities and beating oscillations. *Combust. Flame* **2020**, *212*, 500−509.

(34) Guan, Y.; Liu, P.; Jin, B.; Gupta, V.; Li, L. K. B. Nonlinear time-series analysis of thermoacoustic oscillations in a solid rocket motor. *Exp. Therm. Fluid Sci.* **2018**, *98*, 217−226.

(35) Takens, F.; *Detecting strange attractors in turbulence BT - Dynamical Systems and Turbulence, Warwick 1980*," 1981; 366−381.

(36) "https://www.mathworks.com/help/predmaint/ref/phasespacereconstruction.html#mw_fb22781d-ede1-4802-bd1a-2e0eccf9464a," 2023.

(37) Abarbanel, H. D.; Brown, R.; Sidorowich, J. J.; Tsimring, L. S. The analysis of observed chaotic data in physical systems. *Rev. Mod. Phys.* **1993**, *65* (4), 1331.

(38) Liu, W.; Xue, R.; Zhang, L.; Yang, Q.; Wang, H. Dynamic Response of a Forced Low - Swirl Premixed Flame with Acoustic Excitation. *Flow, Turbul. Combust.* **2021**, *108*, 1139−1157.

(39) Chen, S., "*Flow-induced vibration of circular cylindrical structures*;" Argonne Natl. Lab.(ANL): Argonne,IL(United States), 1985.

(40) Blevins, R.; *Flow-induced vibration*, 2nd edn; Malabar,. 1990.